Proceedings of the ASME 2013 32nd International Conference on Ocean, Offshore and Arctic Engineering
OMAE2013
June 9-14, 2013, Nantes, France

OMAE2013-10940

ON THE GENERATION OF SPATIALLY PERIODIC BREATHER IN A WAVE TANK

Takuji Waseda[1], Hidetaka Houtani[1,2], Katsuji Tanizawa[2]

[1]Graduate School of Frontier Sciences,
the University of Tokyo,
5-1-5 Kashiwanoha, Kashiwa city,
Chiba, 277-8563, Japan

[2]National Maritime Research Institute
6-38-1, Shinkawa, Mitaka-shi,
Tokyo 181-0004, JAPAN

ABSTRACT

Spatially periodic modulational wave train was generated at the National Maritime Research Institute, Actual Sea Model Basin. The 76 m by 36 m basin of depth 4.5 m is surrounded by 382 paddle type wave generators with wave absorbing capacity. Taking advantage of this unique wave basin, we have compared two generation methods, first controlling the wave makers at both upwind and downwind sides and second controlling just the upwind side. The wave generator signal was computed a-priori by High-Order Spectral Method (HOSM hereafter). The HOSM provided temporally non-periodic time series of the unstable wave train as the wave-maker control signal. A number of wave wires located in the tank were used to compare the wave forms between two different generation methods. Our test result indicates that it is not necessary to provide signal at both ends, because the spatial evolution of the wave train remains periodic in space if the wave maker signal is appropriately controlled. The physical experiment and HOSM simulation seem to agree better with high order of nonlinearity.

1. INTRODUCTION

Modulational instability of free surface gravity wave has been studied extensively, theoretically, numerically and physically in the past. The so-called Benjamin-Feir instability (Benjamin and Feir 1967) is a degenerate case of the four-wave resonance and therefore is an outcome of an interaction of spatially periodic wave trains. Because the problem is 2D (1 space + time), one can conveniently apply a coordinate transformation switching space and time (e.g. Groesen and Andonowati 2006). This transformation allows one to generate a modulational wave train that evolves in space by providing temporally periodic signal at the wave maker. Hence the evolution of the wave train should be described by spatial NLS (Nonlinear Schrödinger Equation).

Recent development in the understanding of freak waves in the ocean has shed light on the role of the modulational instability in the evolution of random directional waves. Numerous experimental, theoretical and observational studies provided evidence that the narrowing of the directional spectrum is related to the increased occurrence probability of freak waves, i.e. the freakish sea state (e.g. Waseda et al., 2011 and references therein). However, even for the most likely uni-directional case, the occurrence of freak wave is rather rare (once every few thousand wave periods). Therefore, in order to generate freak wave for a given spectrum in a wave tank, an experiment of a few thousand wave periods is required.

A number of ship accidents near Japan may have occurred during freakish sea state but their direct causes are not known (Waseda et al., 2012). To identify the direct causes of these ship accidents, we would like to reproduce supposedly dangerous waves in the wave tank. To do so, a plausible method is to first conduct a Monte-Carlo simulation of random sea numerically (e.g. Toffolli et al. 2010) and generate the control signal of the wave generator for the desired dangerous wave. Numerical Wave Tanks (NWTs) based on boundary integral methods which models the exact geometry of the wave tank is available but at this point it is unrealistic to conduct a Monte-Carlo simulation of random directional waves for thousands of wave periods. Therefore, a use of a more efficient numerical scheme based on HOSM is proposed. In this paper, we report on the preparatory work generating spatially periodic modulational wave train to evaluate the various wave generation methods based on the HOSM simulation.

2. WAVE GENERATION BASED ON HOSM (HOSM-WG)

In model basins, waves are generated by plunging-type, paddle-type or snake-type wave-makers. In most studies, a Stokes wave is assumed to be generated by a sinusoidal oscillation of the paddle, but in reality, an evanescent wave will be generated to compensate for the imperfect geometry of the

wave-maker. Furthermore, a position-feedback control system is known to introduce spurious free waves at frequencies of bound harmonics (Spinneken and Swan 2009, Schaffer 1996). Although, the existence of bound harmonics is crucial in generating nonlinear wave train, as an introduction of the wave generation method, we assume that a desired propagating irrotational free surface gravity waves can be generated at will.

At the Actual Sea Model Basin (hereafter ASMB) of the National Maritime Research Institute (hereafter NMRI), all four sides of the basin is covered by segmented paddle wave-makers. The wave-maker is controlled based on position-feedback system and is able to be operated in an absorbing mode. Therefore, any sides of the tank can be used to specify the incoming and outgoing wave fields.

Let us first consider how a monochromatic regular wave can be generated in a basin with wave-makers at both ends. Propagating wave in positive x-direction can be expressed as:

$$\eta(x,t) = a_0 \sin(kx - \omega t + \varphi) \quad (1)$$

where a_0 is the wave amplitude, k and ω are the wavenumber and wave frequency satisfying the dispersion relationship $\omega^2 = gk$, and φ is the phase. Suppose the wave-maker is located at x_0, then the wave-maker control signal should be specified as following (note that evanescent modes, bound waves and spurious free waves are ignored for simplicity):

$$H(t;\, x_0) = a_0 \sin(kx_0 - \omega t + \varphi) \quad (2)$$

Similarly, at the end of the tank x_1, where the waves leave the tank, the surface elevation can be expressed as:

$$\eta(t;\, x_1) = a_0 \sin(kx_1 - \omega t + \varphi) \quad (3)$$

However, because the wave-maker is facing inward the tank, the phase change should be reversed. Therefore, the wave-maker signal at the end of the tank should be:

$$H(t;\, x_1) = a_0 \sin(-kx_1 + \omega t - \varphi) = -a_0 \sin(kx_1 - \omega t + \varphi) \quad (4)$$

This is nothing but the wave-maker motion in an absorbing mode. In the ASMB, wave-wires are attached to each paddle to detect the local surface elevation change. Therefore, arbitrary waves that are expected to leave the tank will be absorbed according to (4).

Now, let us consider generating waves that are periodic in space (HOSM-WG). The signals at both end of the tank can be expressed as:

$$\begin{cases} H(t;\, x_0) = a_0 \sin(k_n x_0 - \omega_n t + \varphi) \\ H(t;\, x_0 + L) = -a_0 \sin(k_n (x_0 + L) - \omega_n t + \varphi) \end{cases}$$

or

$$\begin{cases} H(t;\, x_0) = a_0 \sin(k_n x_0 - \omega_n t + \varphi) \\ H(t;\, x_0 + L) = -a_0 \sin(k_n x_0 - \omega_n t + \varphi) \end{cases} \quad (5)$$

where ${\omega_n}^2 = gk_n = g\left(\frac{2\pi}{L} n\right)$ and L is the tank length. Thus when spatially periodic waves are generated in the tank, the wave-maker signal at the end of the tank is identical to the motion of the wave-maker in an absorbing mode, (4).

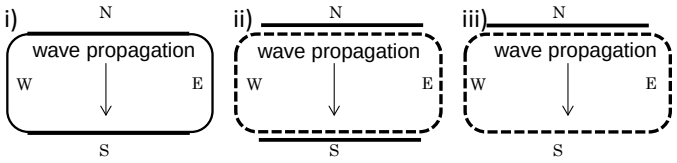

Figure 1: Three wave generation methods were tested: the solid line indicates wave-makers controlled by a given signal; the dashed line indicates wave-makers in an absorption mode. When both solid and dashed lines are present, the wave-makers are controlled by given signal and with wave absorption.

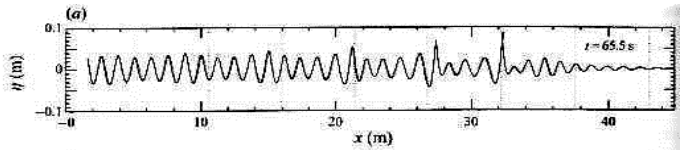

Figure 2: Evolution of unstable wave train with regular wave generation (R-WG) method. Figure cited from Tulin & Waseda (1999).

While the regular wave generation (R-WG) method (2) can be started from still water, HOSM-WG (5) requires that the waves in the entire domain are initialized. It is quite obvious that without the waves initialized in the tank, the wave-makers in both ends will start generating waves propagating inward into an otherwise still water body, and as a result, excitation of standing wave mode in the tank is unavoidable. To circumvent this problem, three remedies were considered and tested at the Actual Sea Model Basin (NMRI). Surface elevation and velocity potential at the domain boundary were extracted from the HOSM calculation and wave-maker control signals were generated accordingly (Figure 1):

i) Control wave-makers at North and South ends by HOSM signal but delay the start of the wave-maker at the end. The wave-makers at the sides are not in motion.
ii) Control wave-makers at North and South ends by HOSM signal and apply absorbing mode for all the wave-makers.
iii) Control wave-maker at the up-wind side only by HOSM signal and apply absorbing mode for all the wave-makers.

Comparing the generated wave forms at the ASMB, it was concluded that the method iii) is sufficient to reproduce spatially periodic wave train. This is good news since in principle this method works for a basin equipped with a wave-maker only in one side of the tank and a beach at the other end. In addition, initialization of the wave field in the tank is not necessary.

In an earlier work, Goullett and Choi (2011) have reproduced numerically a wave field in a uni-directional wave tank using HOSM. When a wave radiate from one side of the tank with R-WG, the amplitudes and phases may evolve in space due to nonlinearity despite the amplitudes and phases of the wave-maker control signal is given as a constant:

$$H(t;\, x_0) = \sum_{i=1}^{N} a_i(x_0) \sin\left(k_i x_0 - \omega_i t + \varphi_i(x_0)\right) \quad (6)$$

An example of a typical wave evolution with R-WG is shown in Figure 2. The wave-maker signal is periodic in time.

However, with HOSM, the amplitudes and phases evolve in time and the wave field is periodic in space. To overcome the discrepancy between wave evolution in space and time, they have terminated the HOSM calculation before the waves wrapped around the computational domain.

On the other hand, when the wave-maker motion is based on HOSM output, the motion will be expressed as:

$$H(t;\, x_0) = \sum_{i=1}^{N} a_i(t) \sin\left(k_{n,i} x_0 - \omega_{n,i} t + \varphi(t)\right) \quad (7)$$

where the amplitudes and phases are time dependent. Note however, that the temporal change is not arbitrary. The key is to control the amplitudes and phases in time, exactly replicating the nonlinear evolution computed in advance by the HOSM.

The success of this method, therefore, would hinge on how well the wave-maker can reproduce the HOSM output. Since there are unknown factors with the overall performance of the wave generation and absorption of the wave-maker and boundary effects in an enclosed basin, a classical unstable wave train due to Benjamin-Feir instability was chosen as a known solution to test the performance of the HOSM-WG.

3. EXPERIMENTAL SETUP

The ASMB of the NMRI is a unique model basin with four sides of the tank surrounded by 382 paddle-type wave generators (Figure 3). The dimension of the tank is 36 m in the North-South direction, 76 m in the East-West direction and 4.5 m in depth. The radius of the rounded corners is 7.7 m. The paddles are independently controllable with given signals as long as their displacements with adjacent paddles are within the specified limit. Wave wire is attached to each paddle surface to detect local surface elevation. The deviation from the control signal will then be absorbed as undesired wave energy. The paddle can be controlled with and without this wave absorption capacity.

In this study, planar waves are generated from the long side of the basin from North to South to minimize possible contamination of the waves because of the rounded corners. Thus, except for the North and South sides, the four corners and the East and West sides are consistently operated with an absorption mode. The generation of waves based on HOSM output was tested with the three methods described in section 2 (Fig. 1). After the trial, it was decided that the South side need not be operated with control signal but be operated in an absorption mode only.

Capacitance type wave wires were placed at about 6 m interval from North to South in the middle of the tank (0.8 m, 6.0 m, 12.0 m, 18.0 m, 24.0 m, 30.0 m and 35.2 m from the North side). Time series were recorded at 100 Hz for 12 minutes.

The wave-generator control signal is given at 0.04 s interval.

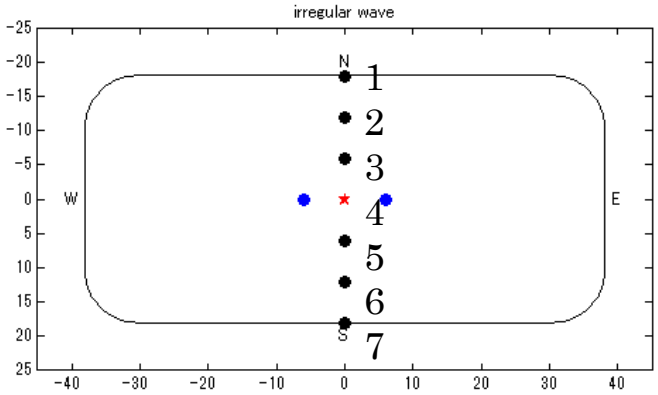

Figure 3: Actual Sea Model Basin of the NMRI. North-West distance is 36 m, East-West distance is 76 m and the radius of the rounded corner is 7.7 m. The wave wires were placed along the middle of the tank from North to South (numbered 1 to 7).

4. HOSM CALCULATIONS

The free surface wave solution is sought for the potential flow with constant depth following the High-Order Spectral Method outlined by West et al. (1987). Following the compact notation of Goullet and Choi (2011), the boundary conditions at the free surface $\zeta(x,y)$ are expressed by velocity potential $\Phi(x,y,z=\zeta)$ recursively to a desired order of nonlinearity M:

$$\begin{cases} \frac{\partial \zeta}{\partial t} = \sum_{n=1}^{M} Q_n[\zeta, \Phi] \\ \frac{\partial \Phi}{\partial t} = \sum_{n=1}^{M} R_n[\zeta, \Phi] \end{cases} \quad (8)$$

The Q_n and R_n are functions of W_n and Φ_n that are expansions of the free surface vertical velocity and free surface velocity potential in nonlinearity orders ζ^n; these functions are defined in Goullet and Choi (2011) and therefore will be omitted here. Because the velocity potential satisfies the Laplace's equation, the vertical gradients are replaced by two-dimensional horizontal gradients and therefore can be solved efficiently in Fourier domain making use of the Fast Fourier Transform (FFT). Hence the rectangular computational domain is regularly discretized by power of 2. Since we are studying uni-directional wave propagation, the computational domain was discretized as 256 by 32 where the second dimension is unnecessary but introduced for numerical reason.

The initial condition of the unstable wave train was specified by linear superposition of Airy waves, the surface elevation and the corresponding velocity potential (omitted):

$$\eta(x) = a_0 \sin(kx) + b_+ \sin\left((k+\delta k)x + \phi_+\right) + b_- \sin\left((k-\delta k)x + \phi_-\right) \quad (9)$$

where $k = 2\pi/\lambda$, $\delta k = k/N_w$, $b = b_+ = b_-$, and $\phi_+ + \phi_- = -\pi/2$. The following parameters were chosen in this study:

λ	ak	N_w	b/a	M
4 m	0.08	9	0.1	3, 4, 5

Therefore, one wave group is formed across the tank width of 36 m. In time, the amplitudes a_0, b_+ and b_- will exchange energy and bound harmonics will grow. However, the wave train will remain periodic in space.

5. RESULTS

The surface elevation and velocity potential extracted from HOSM will nonlinearly grow in time including the bound harmonics but upon generating waves in the wave tank, the wave-maker cannot generate the bound waves. Instead, the bound harmonics will grow instantaneously once the free waves are generated. As a result, unwanted free waves at high frequencies are generated. Other factors will contaminate the waves in the tank as well and therefore it is not apparent how well the HOSM wave forms can be reproduced in the tank.

The evolutions of wave trains from the 7 locations (see Fig. 3) are compared against the HOSM simulation at the nearest grid points, Figure 4. All seven time-series concurrently display temporal cycle of modulation and demodulation, i.e. recurrence, while the differences among the locations are minimal. This comparison suggests that spatially periodic unstable wave train was successfully generated in the ASMB with HOSM-WG. The readers are reminded that the wave-maker signal more or less follows the same time-series displayed in Fig.4. Note, the HOSM simulation was conducted with the order of nonlinearity M=5.

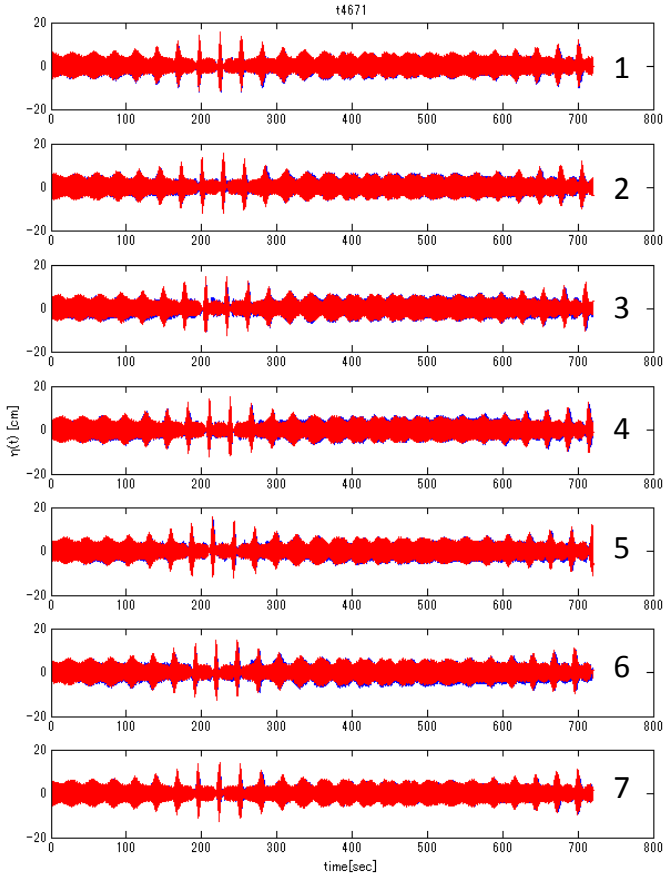

Figure 4: Wave evolution in time from the experiment (blue line) and the HOSM simulation (red line) overlaid on top of each other. The plates from top to bottom correspond to wires 1 to 7 shown in Fig.3.

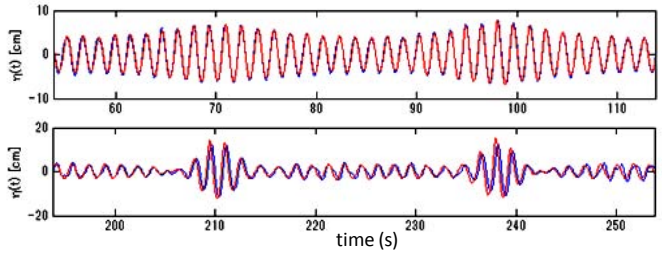

Figure 5: Wave evolution in time from the experiment (blue line) and the HOSM simulation (red line) from wire 4 in Fig.3 for moderate modulation (top) and at peak modulation (bottom).

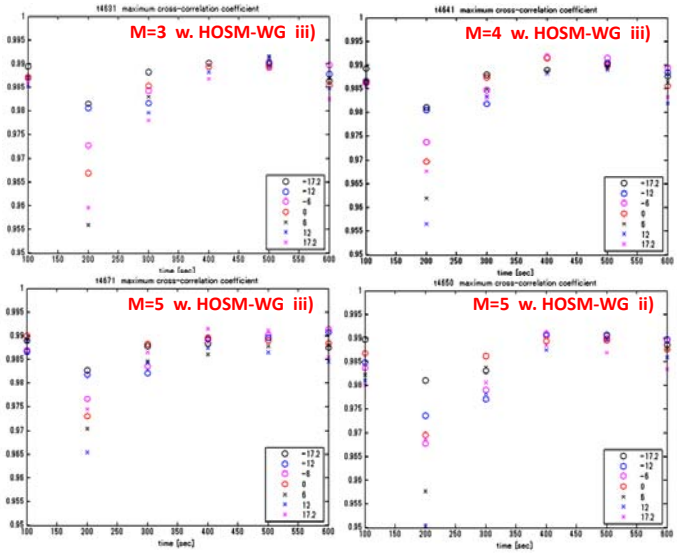

Figure 6: Cross-correlations between the HOSM simulated time-series and the wave-wire records at the ASMB. From top to bottom left figures, the experimental records (at 7 locations) are compared against HOSM simulations with order of nonlinearity from 3 to 5. Bottom right figure shows the comparison with different wave generation method (with wave generation at the end).

Deviation between model and tank experiment stands out when the modulation is largest. The elevation time series are enlarged for an early stage of the evolution (top) and for the peak stage of the modulation (bottom, Figure 5). At the peak stage of the modulation, the numerical solution tends to surpass the elevation of the tank experiment. Phases tend to deviate as well and they are largest at the peak of the modulation.

Cross-correlations (hereafter c.-c.) between the experiment and the model are estimated to quantify the deviation (Figure 6). Initially, the c.-c. are quite high and are between 0.985 and 0.99 for HOSM simulations at orders of nonlinearity M=3, 4 and 5. As the modulation grows, the c.-c. starts to deteriorate to as low as 0.95 or so. As the wave train demodulate, the c.-c. slowly regain their original values, consistent with the observation from the time-series (Fig.4). At the peak of the modulation, the spread of the c.-c. among the wave records is

smallest (0.965~0.98) for the case comparing HOSM simulation with the highest order of nonlinearity (M=5); others had a spread between 0.955~0.98. Thus, to a certain extent, the deviation between the experiment and the HOSM simulation can be explained by the lack of degree of nonlinearity.

The performance of the different wave-generation methods are evaluated with the c.-c. as well. The bottom figures of Fig.6 are the comparisons of the model and experiment for wave-generation methods ii) and iii). There are no remarkable differences as far as the c.-c.. are concerned. This is the reason why we have chosen to control the up-wind wave-makers only while operating the down-wind wave-makers at an absorption mode (section 2).

Overall, the possible reason for the numerical solution to produce higher amplitude than the experiment might be due to neglect of linear evanescent mode and spurious free waves. However, we are aware that the experiment conducted this time had some small mismatch in the control signal which may be responsible for the model-experiment difference.

6. DISCUSSION AND FUTURE WORK

We have successfully generated spatially periodic unstable wave train in a model basin controlling the wave-maker by the HOSM output. In the past, spatial evolution and temporal evolution were conveniently switched so that the nonlinear evolution in space can be expressed, for example, by spatial NLS. This simple coordinate transformation works for uni-directional narrow banded spectrum. However, since our interest is to study evolution of irregular directional wave field in which a simple coordinate transformation cannot be applied, a method to generate spatially periodic wave field is necessary.

As a first step towards generation of spatially periodic directional wave field, we have conducted a simple yet fundamental experiment with unidirectional waves that evolve nonlinearly in time. What is not under our control is the generation of bound harmonics. The wave-maker motion is designed to move following a prescribed position given as a superposition of sinusoids. Therefore, even if we move the wave-maker following the Stokes wave form, a free wave may appear at twice the frequency of the carrier wave but not as a bound wave (Spinneken and Swan 2006). With nonlinearly evolving elevation time-series as a control signal, it is not obvious at all how to control the bound harmonics. Thus, it was not apparent if a wave generation based on HOSM output signal, even for a unidirectional wave, would work. In the case of unstable Stokes wave, we have checked the spectral difference of the HOSM signal and the generated waves (figure 7). When the waves were nearly monochromatic (top figure), the spectrum seems to have been well reproduced for most of the spectral components. On the other hand, as the waves tend to modulate, bound harmonics grow, and larger discrepancies at higher frequencies appeared. Note however, that energy level at bound components tends to be higher for the experimental case (black line, bottom figure) than the HOSM output (red line). The result suggests that in the physical experiment, high-order nonlinearity than the HOSM is in action generating naturally the bound harmonics at high frequency range. In fact, we did not see a large difference among the cases of wave generation using HOSM output at M=3, 4, and 5 degree of nonlinearities. All worked equally well in terms of the wave modulation in time.

Of course, comparison of the local kinematic features of the waves at the peak of the modulation is interesting. The detail comparison is underway and will be reported. Although the result of this preliminary experiment is promising, some fundamental questions remain to be answered. For example, numerically the spectrum is guaranteed to be discrete and therefore nonlinearity in the dispersion relationship will introduce a perturbation in wave frequency. In physical experiment, when the wave-maker oscillates at regular frequency, the nonlinear dispersion results in an increase in wavelength. In principle, since the control signal is from the HOSM output, the generated wave takes into account the wave frequency perturbation. We will check if this is the case in the experiments we have conducted.

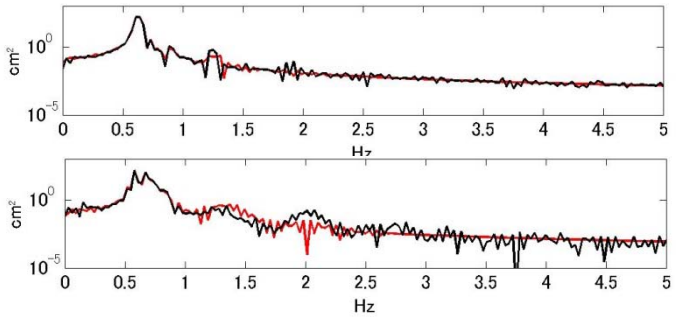

Figure 7: Periodograms of the 30 s long elevation records from the tank experiment (black lines) and the corresponding elevation records from HOSM (red lines). Top diagram is from the initial stage; bottom diagram is from the peak of the modulation.

ACKNOWLEDGMENTS

The basis of the HOSM numerical solver was provided by Dr. Alessandro Toffoli, which is highly appreciated. The first author thanks Dr. Wooyoung Choi for the crucial discussion on the wave generation based on HOSM. This work was supported partially by the Grant-in-Aid for Scientific Research of Japan Society for Promoting Science.

REFERENCES

Benjamin and Feir, 1967, The disintegration of wave trains on deep water, J. Fluid Mech., 27, 417-430.

Goullet, A. & Choi, W., 2011, A numerical and experimental study on the nonlinear evolution of long-crested irregular waves. Physics of Fluids, 23, 016601.

Groesen van, E. and Andonowati (2006) Finite energy wave signals of extremal amplitude in the spatial NLS-dynamics. Physics Letters A, 357 (2). pp. 86-91. ISSN 0375-9601

Toffoli A., Gramstad O., Trulsen K., Monbaliu J., Bitner–Gregersen E., Onorato M., 2010. "Evolution of weakly nonlinear random directional waves: laboratory experiments

and numerical simulations",. J. Fluid Mech., 664, 313–336, DOI:10.1017/S002211201000385X (ERA–A*)

Schaffer, H. A., 1996, Second-order wavemaker theory for irregular waves, *Ocean Engng*, **23 (1)**, 47-88

Spinneken J. and C. Swan, 2009, Second-order wavemaker theory using force-feedback control. Part I: A new theory for regular wave generation, *Ocean Engng*, **36**, 539-548

Tulin and Waseda, 1999, Experimental study of the stability of deep-water wave trains including wind effects, *J. Fluid Mech.*, **401**, 55-84

Waseda, T., M. Hallerstig, K. Ozaki, and H. Tomita (2011b) Enhanced freak wave oc.-c.urrence with narrow directional spectrum in the North Sea, Geophys. Res. Lett., 38, L13605, doi:10.1029/2011GL047779.

Waseda, Tamura and Kinoshita, 2012, Freakish sea index and sea states during ship ac.-c.idents, Journal of Marine Science and Technology, 1-10, doi:10.1007/s00773-012-0171-4

West, B.J., K.A. Brueckner, and R.S. Janda, 1987, A method of studying nonlinear random field of surface gravity waves by direct numerical simulation, J. Geophys. Res., 92, 803–11 824